DD

SW 9432

GANIL

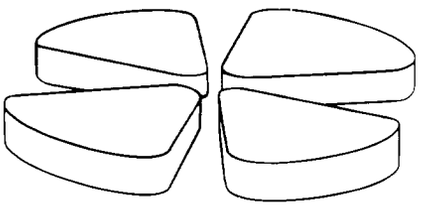

A Cyclotron as a High Resolution Mass Spectrometer for Fast Secondary Ions

G. Auger[1)], W. Mittig[1)], A. Lépine–Szily[1,2)], L. K. Fifield[1,3)], M. Bajard[1)], E. Baron[1)], D. Bibet[1)], P. Bricault[1,4)], J. M. Casandjian[1)], M. Chabert[1)], M. Chartier[1)], J. Fermé[1)], L. Gaudard[1)], A. Gillibert[5)], M. Lewitowicz[1)], M. H. Moscatello[1)], N. A. Orr[1,6)], E. Plagnol[1,7)], C. Ricault[1)], A. C. C. Villari[1,2)], Yang Yong Feng[1,8)]

1. GANIL, BP 5027, 14021 Caen Cedex, France
2. IFUSP-Universidade de São Paulo, C.P.20516, 14098 São Paulo, Brasil
3. Dept. of Nuclear Physics, R.S.Phys.S., Australian National University, GPO Box 4, Canberra, ACT 2601, Australia
4. TRIUMF, 4004 Westbrook Mall, Vancouver, B.C. V6T 2A3 Canada
5. DAPNIA/SPhN, CEN Saclay, 91190 Gif-sur-Yvette, France
6. LPC-ISMRA, Bld du Maréchal Juin, 14050 Caen, Cedex, France
7. IPN Orsay, BP 1, 91406 Orsay Cedex, France
8. Inst. Mod. Phys. Acad. Sinica, No 57 Nanchang Rd Lanzhou, China

GANIL P 94 19

A Cyclotron as a High Resolution Mass Spectrometer for Fast Secondary Ions

G. Auger[1)], W. Mittig[1)], A. Lépine–Szily[1,2)], L. K. Fifield[1,3)], M. Bajard[1)], E. Baron[1)], D. Bibet[1)], P. Bricault[1,4)], J. M. Casandjian[1)], M. Chabert[1)], M. Chartier[1)], J. Fermé[1)], L. Gaudard[1)], A. Gillibert[5)], M. Lewitowicz[1)], M. H. Moscatello[1)], N. A. Orr[1,6)], E. Plagnol[1,7)], C. Ricault[1)], A. C. C. Villari[1,2)], Yang Yong Feng[1,8)]

1. GANIL, BP 5027, 14021 Caen Cedex, France
2. IFUSP-Universidade de São Paulo, C.P.20516, 14098 São Paulo, Brasil
3. Dept. of Nuclear Physics, R.S.Phys.S., Australian National University, GPO Box 4, Canberra, ACT 2601, Australia
4. TRIUMF, 4004 Westbrook Mall, Vancouver, B.C. V6T 2A3 Canada
5. DAPNIA/SPhN, CEN Saclay, 91190 Gif-sur-Yvette, France
6. LPC-ISMRA, Bld du Maréchal Juin, 14050 Caen, Cedex, France
7. IPN Orsay, BP 1, 91406 Orsay Cedex, France
8. Inst. Mod. Phys. Acad. Sinica, No 57 Nanchang Rd Lanzhou, China

May 28, 1994

Abstract

We present the first results from a new method for mass measurements developed using the GANIL coupled cyclotrons, which uses a cyclotron as a high resolution mass spectrometer for fast secondary ions. We report here the results obtained with primary beams of 13.74 MeV/nucleon ^{15}N and ^{12}C, accelerated by the first cyclotron and incident on a Ta target located between the cyclotrons. Reaction products with mass–to–charge ratio of 3 were selected and accelerated by the second cyclotron. The accelerated secondary nuclei were detected in the interior of the second cyclotron using a plastic scintillator located on a radially moving rod. Details of the procedure and results are discussed. When two masses are close enough to be accelerated simultanously by the second cyclotron, the precision in the measurement of the mass difference is better than 10^{-6}.

1 Introduction

The mass of a nucleus is a fundamental property providing the first quantitative information on nuclear binding and structure. Of particular interest are the masses of nuclei far from stability [1] and as such a wide variety of methods of varying precisions have been used to undertake their measurement. These techniques have been coupled to different production mechanisms which range from low energy fusion–evaporation and transfer reactions to high energy fragmentation reactions. In the latter category a number of direct time-of-flight mass measurement techniques have been developed[2–7], in particular around the high resolution magnetic spectrometers SPEG[8] at GANIL and TOFI[9] at Los Alamos.

In these measurements the mass, m, of an ion produced in a nuclear reaction may be determined from the measurements of the magnetic rigidity ($B\rho$) and velocity (v),

$$B\rho = \gamma m v/q \tag{1}$$

where q is the charge of the ion and γ the usual relativistic factor. At GANIL the "exotic" nuclei were produced at beam energies of typically 50–80 MeV/nucleon by projectile fragmentation in a target placed not far from the exit of the second cyclotron. The velocities were subsequently measured over a flight path of 82 meters and the rigidities determined using the high–resolution magnetic spectrometer SPEG. In the TOFI measurements the exotic nuclei were produced via proton induced spallation of a heavy target. Due to the isochronous character of the spectrometer (i.e., the flight-time is independent of the velocity) only a measure of the time–of–flight was required. The mass resolution (FWHM) achieved with these systems is limited by the length of the flight path to $\sim 3 \times 10^{-4}$. In order to extend this method to heavier nuclei and to achieve higher precision for the lighter ones, a substantially longer flight–path is required. Given the physical limitations on a rectilinear flight path, this can best be achieved if the ions follow a spiral path. Motivated by these considerations we have considered[10] the possibility of using the second cyclotron at GANIL as a long flight–path spectrometer for precision mass measurements of exotic nuclei over much of the periodic table. An ion making 250 turns in the cyclotron travels a total flight path of 3.3 km, whence a mass resolution of 5×10^{-6} should be attainable.

It should be noted that the technique of mass detemination using the measurement of the cyclotron frequency in a storage ring has recently been investigated using the ESR at the GSI SIS facility[11]. Additionally, very good precision can be obtained by measuring the cyclotron frequency at very low energy, where the radius of the orbit is very small. If the particles are confined to a small volume a very homogeneous and stable magnetic field may be applied, as in the very high quality measurements recently realized using a Penning trap at ISOLDE[12].

In the present article we will describe results obtained in the acceleration of secondary ions in the second cyclotron at GANIL.

2 Principle of the Method

GANIL(Grand Accelerateur National d'Ions Lourds) consists of a system of three coupled cyclotrons (fig.1) in which highly charged ions from an ECR source are preaccelerated by a small compact cyclotron (C0) before being injected into the first of two identical separated–sector cyclotrons (CSS1 and CSS2). In "standard" operation the accelerated ions emerging

from CSS1 are stripped of electrons in a thin carbon foil before being injected into CSS2 for further acceleration. If this stripper foil is replaced with a much thicker target secondary ions may be produced via nuclear reactions and, rather than the the stripped ions of the primary beam, may be accelerated in CSS2. With a suitable detection system (see Section 3.2) and a calibration based on ions of known masses it is thus possible, in principle, to determine the mass of the secondary ions to high precision.

2.1 Considerations for coupling two cyclotrons

The fundamental cyclotron relation,

$$\frac{B}{\omega/h} = \frac{m}{q} \tag{2}$$

with,

$$\omega = 2\pi f \tag{3}$$

must be obeyed by isochronous ions circulating in *both* cyclotrons. In this relation, f is the radio–frequency (RF) applied to the accelerating cavities, B is the average magnetic field along the orbit of the ion, and h is the beam harmonic, i.e. the number of RF cycles which the ions take to complete one orbit in the cyclotron. At GANIL f is constrained to be the same for all three cyclotrons. Hence,

$$\frac{h_2}{h_1} = \frac{m_2/q_2}{m_1/q_1} \times \frac{B_1}{B_2} \tag{4}$$

The fact that the extraction radius from CSS1, ρ_1, and the injection radius into CSS2, ρ_2, are in the ratio ρ_1/ρ_2=5/2 leads to an additional relation,

$$\frac{h_2}{h_1} = \frac{2}{5} \times \frac{v_1}{v_2} \tag{5}$$

where v_1 and v_2 are the velocities at extraction from CSS1 and at injection into CSS2 respectively. Due to mechanical constraints between C0 and CSS1, h_1=5. Whence,

$$\frac{v_2}{v_1} = \frac{2}{h_2} \tag{6}$$

In the standard mode of operation in which CSS2 is used to increase the energy of the beam extracted from CSS1, $v_1 = v_2$, and hence it follows that h_2=2. Given that the production of secondary nuclei by nuclear reactions between CSS1 and CSS2 will invariably be associated with a loss in velocity, one must consider other solutions to equation (6) for which $v_2 \leq v_1$. These other solutions of v_2/v_1 for which CSS2 can accelerate a secondary beam constitute an ensemble of "magic numbers", v_2/v_1=2/3, 1/2, 2/5, etc. If the reaction does not result in ions with the correct velocity, it can be obtained by use of a degrader of appropriate thickness.

Another possible solution, the operation of two cyclotrons with decoupled RF, has been tested using the SARA cyclotrons[19] at Grenoble. This method, however, results in intensity losses and requires the determination of the total number of turns executed by the ions.

2.2 Acceleration of secondary ions in CSS2

2.2.1 Precision of the method and calibration

Consider two nuclei with slightly different masses, m and $m + \delta m$. During the acceleration process the heavier of the two nuclei will lag behind the other and, for sufficiently small δm, the accumulated difference in the time–of–flight, δt, will be proportional to δm, i.e.,

$$\frac{\delta t}{t} = \frac{\delta m}{m} \tag{7}$$

After N_T turns at harmonic h the total time–of–flight t and the total phase Φ_{total} at f=13MHz (T_{HF}=77ns) are,

$$t = 77 \times h \times N_T \tag{8}$$

$$\Phi_{total} = 360^o \times h \times N_T \tag{9}$$

The phase difference $\delta\Phi$ is defined as,

$$\delta\Phi = \delta t \times (\frac{360^o}{T_{HF}}) \tag{10}$$

As an example, taking typical values of $h = 3$ and $N_T = 250$ one finds that,

$$\frac{\delta m}{m} = 1.7 \times 10^{-5} \times \delta t(ns) \tag{11}$$

A time resolution of $\sim 300ps$ is readily attainable between start and stop detectors, resulting in a mass resolution of,

$$\frac{\delta m}{m} = 4 \times 10^{-6} \tag{12}$$

For nuclei with sufficiently close mass–to–charge ratios, m/q, the above relation (7) between δm and δt evidently forms the basis of the calibration procedure. If they are accelerated simultaneously, then eq. 7 allows the precise determination of the "unknown" mass from the "reference" mass – the "reference nucleus" has a well known m/q and the "unknown", a mass which we wish to measure. However, the acceptance of the cyclotron for the simultaneous acceleration of different ion species is $\sim 10^{-4}$. Consequently, if the fractional difference in the mass–to–charge ratio of the two nuclei is larger than 10^{-4} they will not be accelerated simultaneously with the same magnetic field B in CSS2 (this is the case for many light ions) and some sort of sequential process such as changing the magnetic field or RF is required.

The calibration of the time–of–flight or phase against magnetic field B can be obtained by accelerating the same nucleus and measuring the phase variations after applying small changes in B. A change in the magnetic field, δB, results in the same time–of–flight for the nucleus with mass $m + \delta m$ as for the one of mass m with a field B applied, if the particles have the same trajectories.

The variations in B (or in frequency) are directly related to the mass differences between the nuclei. If the two nuclei have the same trajectory and execute the same number of orbits in the second cyclotron, then equation (2) applies directly and one has,

$$\frac{\delta B}{B} = \frac{\delta t}{t} = \frac{\delta m}{m} = \frac{\delta\Phi}{\Phi_{total}} \tag{13}$$

In practice, however, this simple linear relation (eq. 13) comparing phases measured with different magnetic fields in CSS2 or with different frequencies in the cyclotrons will not be satisfied rigorously, as will be demonstrated in the following sections.

3 Experimental procedure

The experimental measurements were executed in three different stages, with different primary beams and different objectives.

3.1 Acceptance of CSS2

The first goal was to perform an experimental study of the acceptance of CSS2 by measuring the transmission of a relatively intense "secondary" beam after injection and acceleration through the first ~50 turns in CSS2. A primary beam of 9.14 MeV/nucleon $^{13}C^{3+}$ was extracted from CSS1 with an intensity of 300 nA_e and the intense "secondary" beam was the completely stripped ^{13}C ions, slowed down to v_2=$v_1 \times 2/3$ using a rotating, cooled 30 mg/cm^2 ^{nat}C target placed between CSS1 and CSS2. Due to the relatively low incident energy and high beam intensity the energy dissipation in the target was very high ($\sim 6W$), hence the need for the cooled, rotating target.

Variable horizontal and vertical slits located 1.2 m downstream from the target and variable horizontal slits located after the analyzing dipole of the injection line provided for the variation of the angular emittance ($\delta\theta$ and $\delta\varphi$) and momentum range (δp) respectively of the "secondary" beam. The acceptance of CSS2 was determined by the measurement of the beam intensity of the injected and accelerated "secondary" beam in CSS2 as a function of these parameters. The beam intensities were measured using Faraday cups before the target, before injection and on radial probes intercepting the beam during the first turn in CSS2.

The angular and momentum acceptances were found to be,

$$\delta\theta = \pm 5.4 mrad \tag{14}$$

$$\delta\varphi = \pm 10 mrad \tag{15}$$

$$\frac{\delta p}{p} = \pm 0.7\% \tag{16}$$

These are in good agreement with the expected values and demonstrate that CSS2 has a relatively high acceptance. The total transmission of the beam as measured before the target and during the first orbit was 1.8%. This value is 40% lower than the calculated transmission taking into account the angular and energy straggling in the target – quite good agreement considering the experimental uncertainties. Some difference may be introduced by the very long inflection channel, that may introduce a coupling between the cut in the θ and δ acceptances.

3.2 Particle detection for the secondary beams

Three different detector arrangements were used for the detection of the secondary ions (fig. 1).

- The reaction products were detected and identified using a two element silicon detector telescope (50 and 300 μm) located after the analyzing dipole in the injection line of CSS2. A "stop" signal from the telescope provided for a time–of–flight measurement relative to the cyclotron RF. This, associated with the energy–loss, ΔE, and energy, E, measurements provided for the unambiguous identification of all reaction products. This telescope could be inserted into or withdrawn from the beam path: the latter being the case during the injection and acceleration of the secondary ions.

- A micro–channel plate detector was located in the injection line of CSS2, just before the entry into the cyclotron. It was used to provide a "start" signal for the measurement of the total time–of–flight through the cyclotron. This measurement is important when comparing different nuclei as it may be used to verify if the same number of turns have been executed by each. Its use was, however, of limited value in practice as the secondary ions were stripped of their electrons in the thin aluminium coated ($20\mu g/cm^2$) mylar foil ($60\mu g/cm^2$) of the detector. The resulting modified m/q values could not as a result be accelerated by the second cyclotron. Thus it was mainly relegated to use as a control for measuring directly the number of turns executed by a certain species.

- The detection of the secondary ions after acceleration by CSS2 was performed using a plastic scintillator (Pilot–U) mounted on a radial probe and attached to a light–guide which was in turn connected to a bunch of optical fibers[20] with a length of 10 m. The optical fiber bunch was connected at the exterior of the cyclotron to a photomultiplier. The plastic scintillator was mounted on the radially moving rod of the above mentioned probe and the radial position could be varied from a distance to the center of the cyclotron of 1250 mm to 3020 mm. The latter distance corresponds to a position just prior to extraction from CSS2. In fig. 2 a typical example of a Energy versus Phase ($\delta\Phi$) spectrum is displayed for which the radial position was varied over the previously noted limits.

  It should be noted that, due to its interceptive character, any detector used inside the cyclotron must have a inactive inner edge much narrower than the spacing between adjacent orbits (5–6 mm). The Pilot–U detector fulfilled this requirement having no insensitive area presented to the beam. Additionally it provided a very fast timing signal and an energy measurement of limited resolution. The function of this detector was to provide a "stop" signal for the time–of–flight or phase measurement. During the actual measurements it was used in conjunction with the RF signal of the cyclotron. The energy signal, due to the limited resolution could not be used for unambiguous Z identification, but did provide useful indications for low–Z ions.

4 Results of the test measurements

4.1 Mass measurements with changes in the magnetic field

For these measurements a primary beam of $^{15}N^{4+}$ with the maximum available energy of 13.74 MeV/nucleon and an intensity of 2.4 $\mu A_e$was extracted from CSS1 and used to bombard a rotating, cooled 132 mg/cm^2 Ta target. The accelerating cavities were operated at f=13.45 MHz.

In fig. 3 the ΔE–E spectrum obtained using the silicon detector telescope is presented whereby the enormous variety of reaction products present, even after selection by the analyzing dipole, is clearly apparent. Indeed, even at such a relatively low beam energy the very neutron-rich nucleus ^{11}Li could be observed. From the measured production rate, using very limited acceptances and an attenuated primary beam, it is expected that with 2.4 μA_e (the maximum permitted beam current) and the full acceptance for injection into CSS2, a production rate of 0.8 count/minute of ^{11}Li could be attained.

4.1.1 Acceleration of secondary ions with A/q=3.0 in CSS2

Nuclei with A/q=3.0 - $^{15}N^{5+}$, $^{12}B^{4+}$, ^{12}Be, ^{9}Li, ^{6}He etc - were accelerated in CSS2 after being slowed down to v_2=$v_1/2$ prior to injection using the rotating, cooled Ta target. The second cyclotron was tuned with the fairly intense $^{15}N^{5+}$ beam and the isochronism was verified and optimized by varying the radial position of the plastic scintillator.

The m/q values of the ions are displayed in Table I as compared to the reference mass $^{15}N^{5+}$ and defined by the following equation,

$$\frac{\delta(m/q)}{m/q} = \frac{(m/q(^{A}_{Z}X^{q+}) - m/q(^{15}N^{5+})}{m/q(^{15}N^{5+})} \tag{17}$$

The calibration of the phase ($\delta\Phi$, relative to the RF), against magnetic field was obtained by measuring the phase (time–of–flight) of the beam for slightly different ($\sim 10^{-5}$) values of the magnetic field B of CSS2. The magnetic field of CSS2 was determined by making 10 measurements at the same field setting using a Nuclear Magnetic Resonance (NMR) probe at a radial distance of 1700mm. On each occasion the value was logged only after the the NMR reading had stabilized. The relative error of the locally measured B was around 6×10^{-7}.

4.1.2 Ions not accelerated simultaneously.

The switch from the primary beam to secondary beams with A/q=3.0 was made by discrete changes in B, predicted using eq. 13., in order to allow the $^{12}B^{+4}$, ^{12}Be, ^{9}Li and ^{6}He ions to be accelerated in CSS2 and to arrive at the plastic scintillator with phases similar to that of the primary beam $^{15}N^{5+}$. During this process the trim–coils were not readjusted and the isochronism was not remeasured.

The masses of the secondary nuclei can be calculated from eq. (13) , comparing B values corresponding to the same phase as shown in fig. 4. Here the phase $\delta\Phi$ is plotted against magnetic field for the reference nucleus $^{15}N^{5+}$ and for the "unknown" nuclei ^{9}Li and ^{6}He.

In Table II the results for several nuclei arriving at the plastic scintillator at a distance of 3000mm from the center of CSS2 are tabulated. The last column shows the difference between the measured and tabulated[21] values of m/q which are seen to agree within $\sim 10^{-5}$ - the discrepancy increasing for increasing mass differences when the different nuclei are not accelerated simultaneously. The reason for this discrepancy is well understood and will be discussed in section 5.

4.1.3 Ions accelerated simultaneously.

The relative difference between the m/q values of ^{9}Li and ^{6}He is 1.7×10^{-4} and consequently they can be accelerated simultaneously in CSS2. In fig. 5 the phase (time–of–flight) spectra of the ions arriving at the plastic scintillator at 3000 mm are displayed. Two peaks are clearly observed corresponding to ^{9}Li and ^{6}He. From the peak width in fig. 5 the mass resolution may be calculated: the σ (Gaussian) of the ^{6}He peak corresponding to a resolution of 5×10^{-6}. The final precision of the method is, of course, better than this and is dependant on the statistics ($\sigma/\sqrt{N}$).

In the last line of table II the measurements for ^{6}He and ^{9}Li (nuclei which are accelerated simultaneously) are compared. Their phases (time–of–flights) were measured at the same time, with the same B, the same initial phase and the same frequency. The mass difference can thus be calculated from eq.13 by comparing values of B which correspond to the same

phase ($\delta\Phi$). The difference in m/q agrees with the tabulated difference to within 9×10^{-9}, with a precision of around 8×10^{-7} .

It may be concluded, therefore, that when two nuclei are accelerated simultaneously with the same initial phase and the same magnetic field (even if not uniform), a very high precision in the measured mass difference (and effectively in the mass of one if the other is a reference) can be obtained.

4.2 Mass measurements with changes in the frequency

A primary beam of $^{12}C^{3+}$ with an intensity of 400 nA_e and the maximum available energy of 13.74 MeV/nucleon was extracted from CSS1 and used to bombard the Ta target which was used for the production and slowing–down of the secondary ions. The accelerating cavities were operated at f=13.45 MHz. In this series of measurements the interest lay in secondary beams with A/q=3.0 and velocities $v_2 = 2 \times v_1/3$ ($h_2 = 3$). The isochronism of CSS2 was measured and optimized with the fairly intense, slowed–down primary beam $^{12}C^{4+}$ (A/q=3.0) by varying the radial position of the plastic scintillator.

Our objective was acceleration in CSS2 of the secondary beams with A/q=3.0 – $^{12}C^{4+}$, $^{12}B^{4+}$, ^{12}Be, ^{9}Li and ^{6}He – by changing the frequency, instead of the magnetic field, as was done previously. This change in frequency was automatically accompanied by a corresponding change in the magnetic field B in C0 and CSS1.

Frequency changes for CSS2 are, in fact, rather time consuming and in practice only an increase can be made in a relatively short period. However, if we examine eq. (2) it can be seen that an increase in frequency corresponds to a decrease in m/q. Unfortunately, the other nuclei with A/q=3.0 which we wish to accelerate have larger values of m/q. Thus by starting with the reference nucleus $^{12}C^{4+}$ these nuclei cannot be reached by simply increasing the frequency. For this reason we combined frequency and magnetic field variations successively.

After tuning CSS2 and optimizing the isochronism with the $^{12}C^{4+}$ beam, the magnetic field was increased by a factor of 1.00314808 at constant frequency in order to accelerate the ^{9}Li and ^{6}He ions. The phase $\delta\phi$ (with respect to the RF) of the ^{9}Li and ^{6}He ions at 3000 mm as a function of the RF is presented in fig. 6. The measured m/q difference agrees with the tabulated value to within 6×10^{-7}. Once again it may be seen that when the nuclei are accelerated simultaneously, with the same magnetic field and frequency, their mass difference may be determined to a a very high precision.

We then performed a frequency change in order to accelerate the ^{12}Be secondary ions. If we compare the frequencies for which the ^{12}Be and the ^{6}He ions arrive at the scintillator with the same phase, the mass difference may be calculated using equation (13). The m/q determined in this manner differs from the tabulated value by 4.7×10^{-5}, of the same order of magnitude as the discrepancy found for the method utilising the variation of the magnetic field.

The total time–of–flight can be calculated using eq. (13) and the time–of–flight differences δt due to the differences in m/q,

$$t = \delta t/(\frac{\delta(m/q)}{m/q}) \tag{18}$$

It may be noted, that this method gives about the same total time–of–flight as the direct measurement using the micro–channel plate detector to provide a "start" and the plastic scintillator at 3000mm a "stop" signal.

5 Difficulties in the experimental method.

5.1 Isochronism, changes in the main magnetic field and in the radio frequency

The measurement of the phase as a function of radius, performed by varying the radial position of the plastic scintillator (see fig.2) is usually referred to as the verification of the isochronism. Deviations from isochronism are corrected by tuning the trim–coils of the cycloton accordingly. Perfect isochronism corresponds to a constant phase along the radius. A quite good isochronism was obtained for the degraded primary beam $^{12}C^{4+}$ (see fig.2).

The radial phase variation has also been determined for some of the secondary ions with A/q=3.0 ($^{9}Li^{+3}$, $^{6}He^{+2}$ and $^{12}Be^{+4}$) which were accelerated in CSS2 by measuring the phase or relative time-of-flight (with respect to the RF signal) at different radial positions. The magnetic field in CSS2 was changed in order to switch from the $^{12}C^{4+}$ beam to the ^{9}Li and ^{6}He secondary beams following eq. (13). The trim–coils were not adjusted when the main field was changed.

The schematic variation of the phase with radial position measured for the ^{6}He, ^{9}Li and ^{12}Be secondary beams is displayed in fig. 7. It may be clearly seen that good isochronism in the primary beam did not result in good isochronism for the secondary beams. The phase variations with radius, mainly at the beginning of the trajectory are surprisingly large: 57^o for $^{6}He^{+2}$ and 77^o for $^{9}Li^{+3}$ (one RF period being defined as a 360^o phase variation). It should be noted that a phase variation of $\geq 90^o$ results in the deceleration and subsequent loss of the beam.

The cause for these large phase deviations is of a magnetic nature. The change of about 3×10^{-3} in B is relatively large and not uniformly established in the interior of CSS2. Usually, due to saturation effects, when the current in the main coil is increased the field becomes more intense at small radii and less intense at large radii. Thus, to regain isochronic orbits after a change in the main field B, the trim-coils must be readjusted in order to correct for the non–uniformities. The phase deviations, first toward negative phases (B too intense) and after toward positive phases (a weaker B) as the radius increases, can be understood in terms of these non–uniformities in the magnetic field.

It is clear now that the comparison of the final phases of different nuclei, even if their initial phase was the same, obtained with a discrete change in B without corrections applied to the trim–coils, cannot furnish a precise determination of the mass difference using the simple linear relation of eq.13.

A simple calculation of the phase as a function of radius and mass has been performed supposing that the radial non-uniformities in the magnetic field have linear, quadratic and cubic terms. With field non–uniformities whose order of magnitude is $\sim 10^{-4}$ of the average field, a reasonable agreement was obtained for ^{6}He and ^{9}Li by assuming that the relative m/q difference (eq. 17) between them is 1.7×10^{-4}. (see fig.7)

The ^{12}Be beam was accelerated by making a change in the frequency. This change does not necessitate a different magnetic field but does change the initial phase of the particles – it cannot be supposed that the ^{12}Be ions had the same initial phase as ^{6}He. We included in the calculations the change in frequency and m/q and for the same magnetic field but somewhat different initial phase and could reproduce quite well the phase variation of ^{12}Be (see fig.7).

If the measured phase is compared to the calculations, the mass of ^{12}Be compared to that of ^{6}He may be determined. In this manner a mass is obtained which agrees with the

tabulated value to within 4×10^{-6}, an improvement of a factor of 10 in the precision found before.

In the case of a frequency change, the magnetic field remains unchanged and no phase variations appear due to the field changes. The initial phase is, however, now unknown and the final phase obviously depends on the initial phase. However, the calculation of the phase variation with radius can furnish this information and allow this method to be employed for light nuclei.

5.2 Precession, betatron oscillations and the overlap of trajectories.

The total time–of–flight of the beam could be measured between the micro–channel plate detector and the plastic scintillator. This measurement revealed the existence of several peaks (up to four) in the time–of–flight spectra, implying the presence of several orbits corresponding to different numbers of turns at the same radial probe position. This effect can have two origins:

- One is the precession of beam bunches resulting from imperfect injection which results in the accumulation of trajectories at regular distances (12 turns), whereby several orbits corresponding to different numbers of turns can be located in close proximity to each other.

- The other, the overlap of several trajectories corresponding to different numbers of turns at the same radial position, is a complex phenomenon related to the emittance (radial and longitudinal) of the injected beam bunches, the time variation (sinusoidal) of the accelerating electric field and the properties of an isochronous magnetic field.

This second effect could be minimized by an optimization of the initial RF phase Φ_o. The variation of the total time–of–flight of the degraded primary beam with the initial phase was measured and it was verified that at 3020 mm and for Φ_o around 4.4^o, the effect of the overlap of several trajectories disappeared – this being evidenced by the presence of only one peak in the time–of–flight spectrum. The phase window in which only one peak is present is very restricted – less then 20^o. Variations of the order of $\pm 10^o$ in the inital RF phase around the optimal value produced double peaks.

If the initial RF phase is not exactly at the optimal value, any small changes in the magnetic field B can result in the overlap or crossing of trajectories and consequently the appearence of several peaks in the time–of–flight spectrum. Such behaviour is depicted in fig. 8.

In the case of light nuclei the problem of precession and overlaping orbits does not seriously affect the measurements. In the case of heavier nuclei, however, which are accelerated simultaneously and for which no change in B or f is required (due to the presence at the same settings of reference nuclei), the appearence of multiple peaks as discussed above, can pose a serious problem. This behaviour must therefore be avoided by paying particular attention to the injection conditions for CSS2 and by optimizing the initial phase of the accelerating RF voltage.

6 Conclusions

Several conclusions can be drawn from the tests performed and analysed in this paper:

- In the situation were the nuclei are accelerated simultaneously, are subject to the same magnetic field along their paths and have the same initial phase, the "unknown" mass could be determined with a precision of better than 10^{-6}.

- It was verified that changes in the magnetic field induce relatively large non-uniformities which result in large phase variations and, consequently, in a limited precision in the mass determination. The method involving changing the magnetic field B thus does not represent a very precise and reliable method.

- The method employing frequency (RF) changes, whilst being more time-consuming, is more precise. It has the advantage of not modifying the isochronism of the ions when the switch is made from one mass to another as the magnetic field is not changed. However, it does present the serious disadvantage of losing the initial phase of the injected ions. This may be circumvented through calculations of the phase variation. Using such a technique a precision of 4×10^{-6} has been demonstrated.

In summary, much experience and a good understanding of the problems involved with the acceleration of secondary ions in a cyclotron has been obtained. The methods developed here may also serve as powerful tools for tuning secondary or highly attenuated primary beams.

7 References

1. C. Détraz and D.J. Vieira, Ann. Rev. Nucl. Part. Science, 39 (189) 407
2. A. Gillibert et al, Phys. Lett. B176 (1986) 317.
3. D. J. Vieira et al, Phys. Rev. Lett. 57 (1986) 3253.
4. A. Gillibert et al, Phys. Lett. B192 (1987) 39.
5. J. Wouters et al, Z. Phys. A331 (1988) 229.
6. X. L. Tu et al, Z. Phys. A337 (1990) 361.
7. N. A. Orr et al, Phys. Lett. B258 (1991) 29.
8. L. Bianchi et al, Nucl. Instr. Meth. A276 (1989) 509.
9. J. M. Wouters et al, Nucl. Instr. Meth. B26 (1987) 286.
10. G. Auger et al, 14th Europ. Conf. on Nucl. Phys. Bratislava, oct. 1990. and P. Bricault et al, Proc. 13th Int. Conf. on Cyclotrons and their applications, Vancouver, 1992, pp 158-161.
11. H. Geissel et al, Phys. Rev. Lett. 68 (1992) 3412.
12. H. Stolzenberg et al, Phys. Rev. Lett. 65 (1990) 3104.
13. S. Khan, et al, Phys. Lett. 156B (1985) 155.
14. B.M. Young et al, Phys. Rev. Lett. 71 (1993) 4124.
15. R. Gilman et al, Phys. Rev. C30 (1984) 958.
16. A. Huck et al, Phys. Rev. C31 (1985) 2226.
17. K.S. Sharma et al, Phys. Rev. C44 (1991) 2439.
18 T. Otto et al, Nucl. Phys. A567 (1994) 281.
19. D. Barnéoud et al, 28th Eur. Cycl. Progr. Meeting, Jyvas, sept.1993.
20. D. Lhuillier, Rapport de stage DEA, University of Caen (1993).
21. G. Audi and A. H. Wapstra The 1993 Atomic Mass Evaluation, Nucl. Phys. A565 (1993) 1.
22. G. Munzenberg et al, Z. Phys. A328 (1987) 49.

8 Figure Captions

Fig.1 Schematic diagram of the three cyclotron complex of GANIL. Indicated are the locations of the target and various detectors used in the present work.

Fig.2 Energy versus phase for $^{12}C^{4+}$ ions detected by the plastic scintillator. The latter being the time–of–flight relative to the RF transformed into phase using eq. (10). The spectrum was obtained by varying the radial position of the the probe – the increasing energy corresponding to an increasing radial position. The resulting isochronic curve has been used to define the zero for the determination of the phase.

Fig.3 $\Delta E - E$ spectrum obtained using the silicon detector telescope demonstrating the broad range of secondary ions produced by the ^{15}N primary beam in interactions with the Ta target.

Fig.4 The phase variations of the "reference" nucleus $^{15}N^{5+}$ and those of the "unknown" nuclei ^{6}He and ^{9}Li detected using the plastic scintillator at 3000 mm and obtained by changing the magnetic field. The magnetic fields were compared and eq.13 was used to determine the "unknown" masses (see text).

Fig.5 $E \times \delta\Phi$ spectrum for ^{6}He and ^{9}Li when accelerated simultaneously and detected at 3000 mm using the plastic scintillator.

Fig.6 The phase variations for ^{6}He and ^{9}Li nuclei obtained using the method involving frequency changes (see text).

Fig.7 Schematic representation of the isochronic curves for some secondary beams. The crosses represent the phases relative to the cyclotron RF at number of discrete radial positions of the plastic scintillator. The solid lines are results of calculations of the phase variation.

Fig.8 Phase for the $^{15}N^{5+}$ degraded primary beam as measured at a radial position of 3000mm (using the plastic scintillator) as a function of the magnetic field (in arbitrary units). Small changes in B ($\sim 10^{-5}$) produce not only a variation in the phase, but also double and triple peaks.

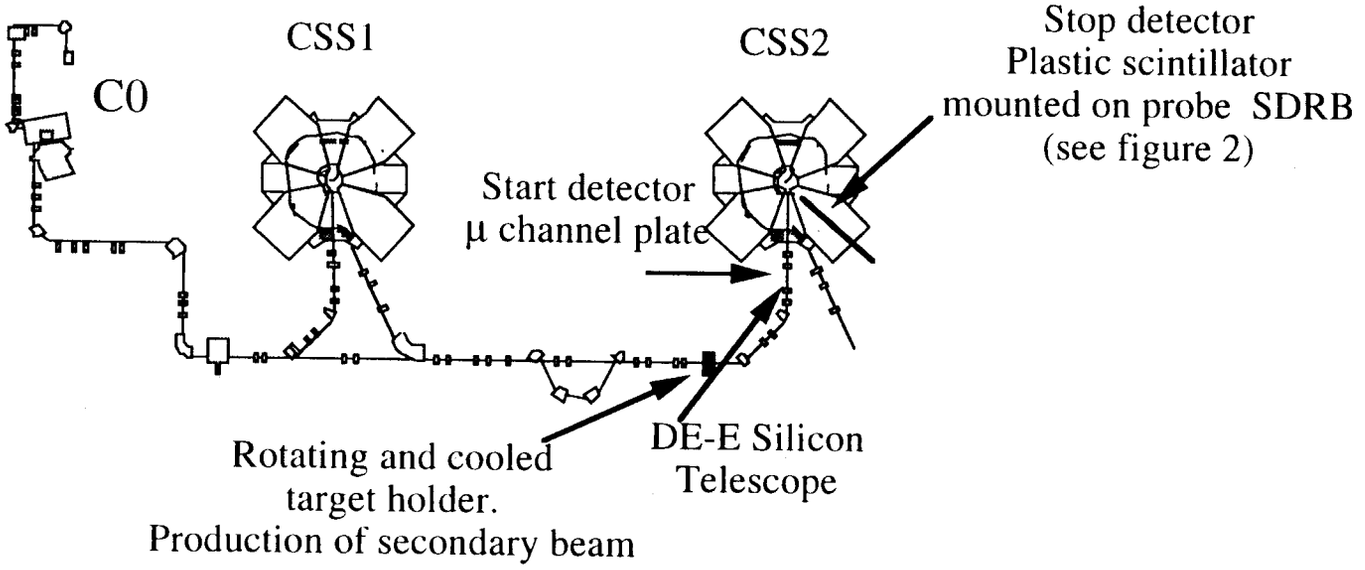
C0
CSS1
CSS2
Stop detector
Plastic scintillator
mounted on probe SDRB
(see figure 2)
Start detector
μ channel plate
Rotating and cooled
target holder.
Production of secondary beam
DE-E Silicon
Telescope

Fig 1

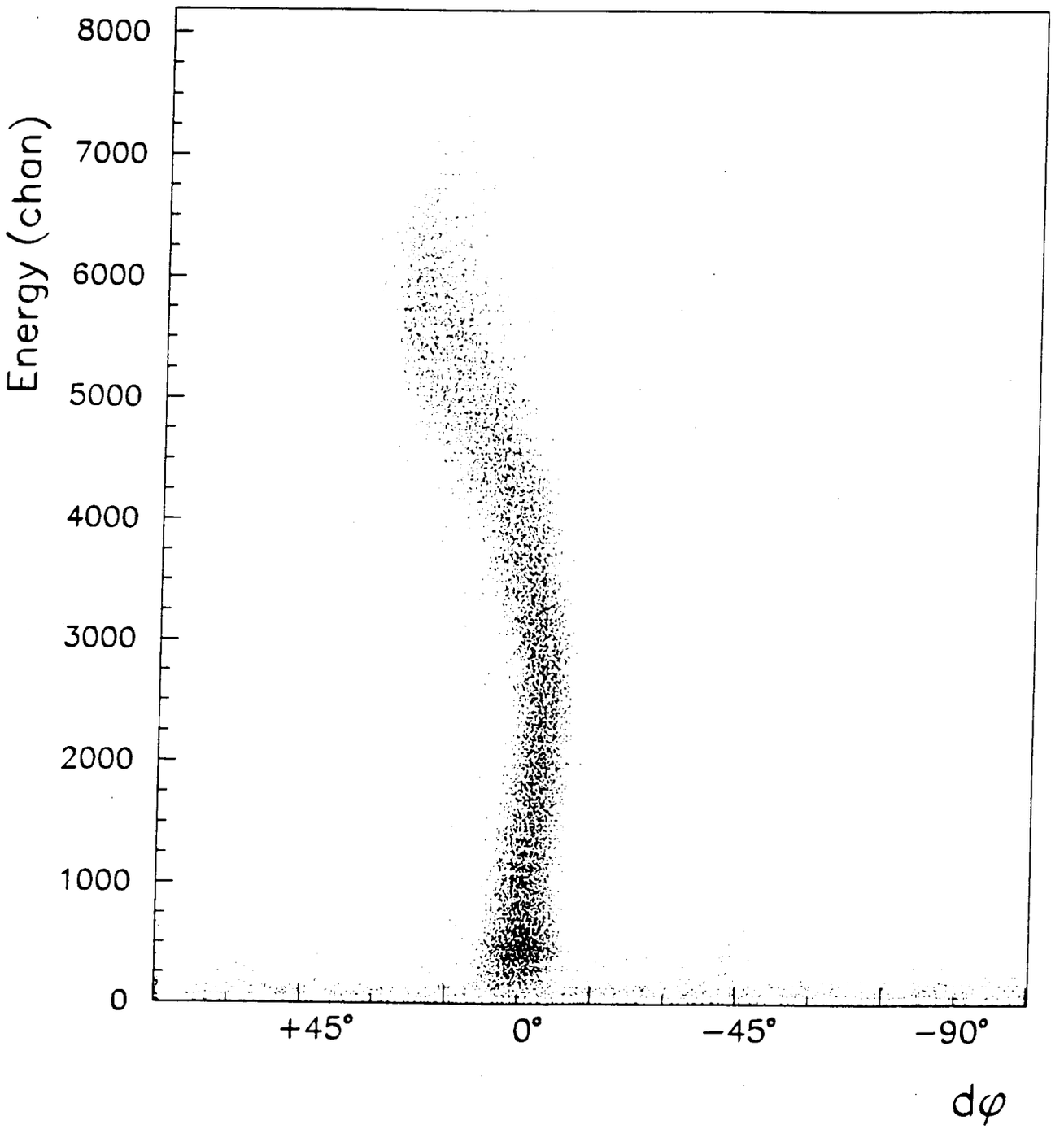
8000
7000
6000
5000
4000
3000
2000
1000
0
Energy (chan)
+45°
0°
−45°
−90°
dφ

Fig. 2

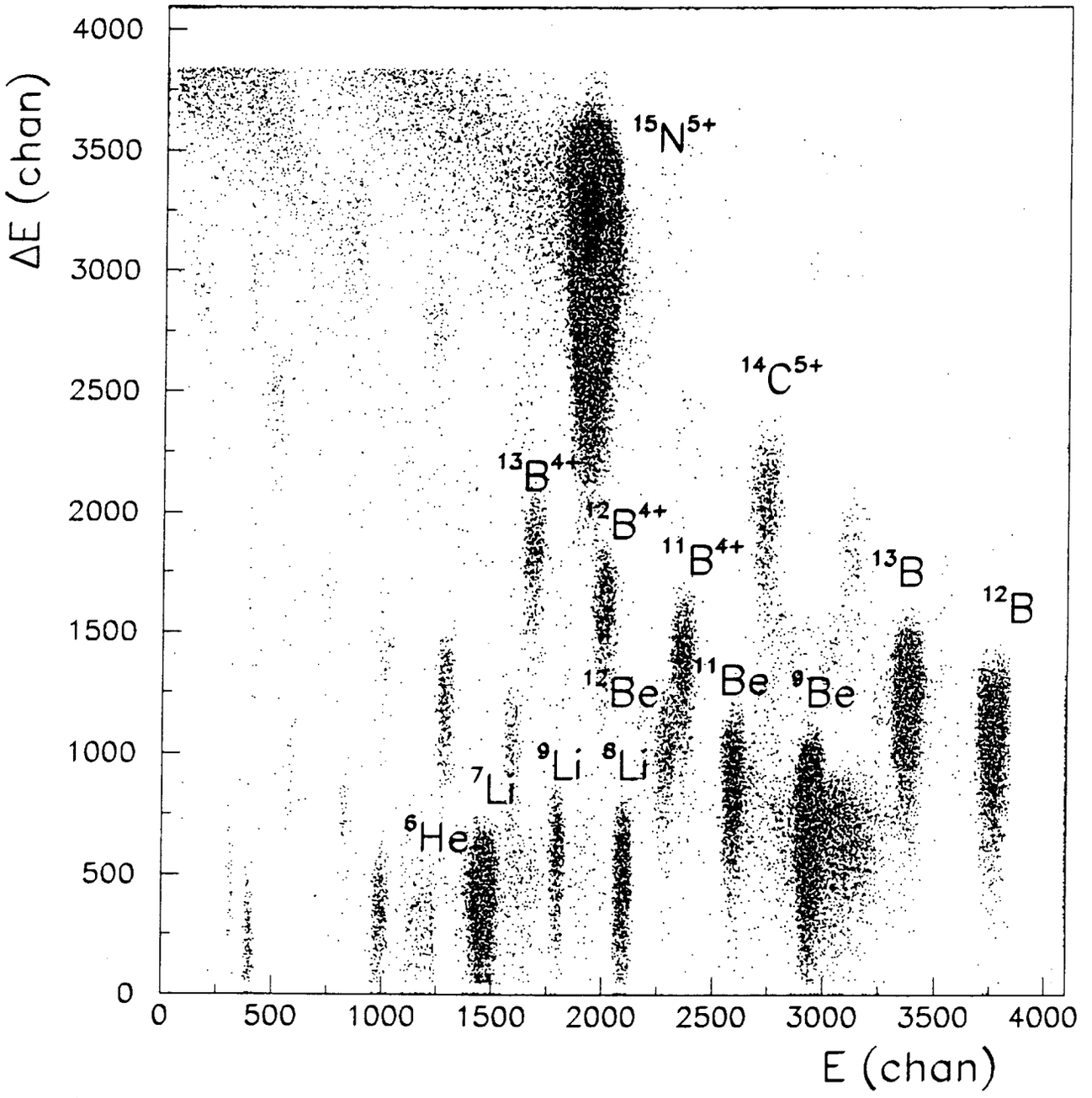
ΔE (chan)
E (chan)
0
500
1000
1500
2000
2500
3000
3500
4000
$^{15}N^{5+}$
$^{14}C^{5+}$
$^{13}B^{4+}$
$^{12}B^{4+}$
$^{11}B^{4+}$
^{13}B
^{12}B
^{12}Be
^{11}Be
^{9}Be
^{9}Li
^{8}Li
^{7}Li
^{6}He

Fig. 3

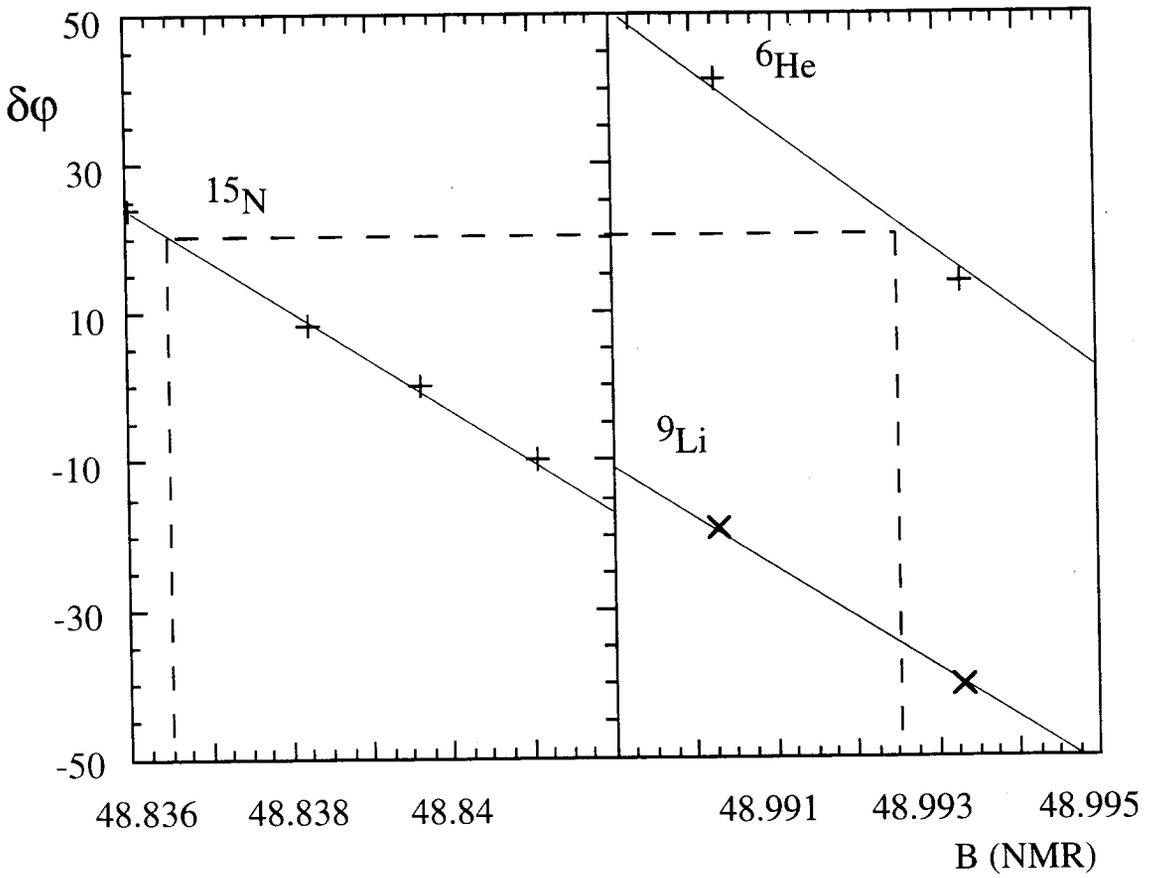
50
δφ
30
10
-10
-30
-50
15N
6He
9Li
48.836
48.838
48.84
48.991
48.993
48.995
B (NMR)

Fig. 4

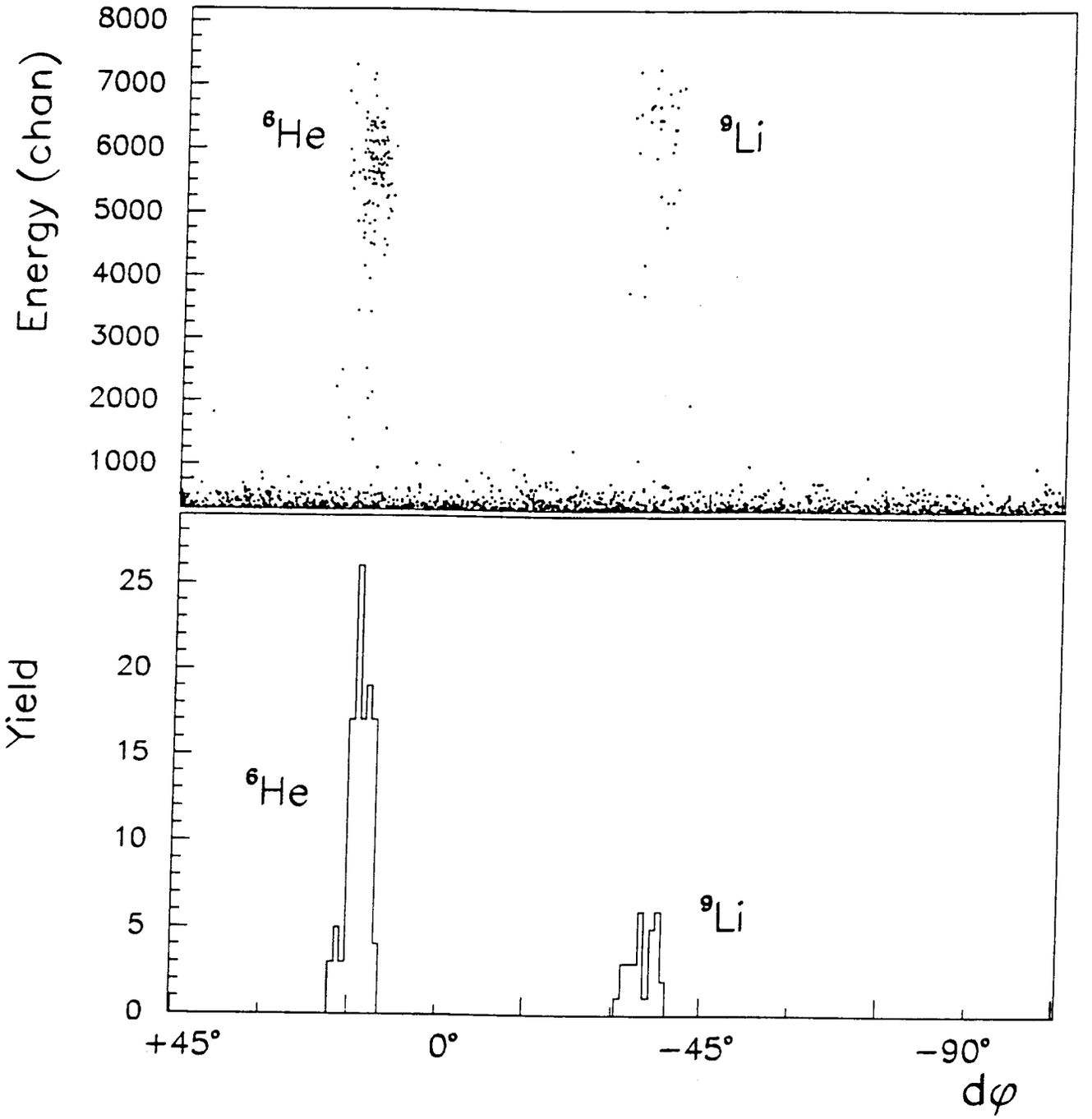
Energy (chan)
8000
7000
6000
5000
4000
3000
2000
1000
^{6}He
^{9}Li
Yield
25
20
15
10
5
0
^{6}He
^{9}Li
+45°
0°
−45°
−90°
dφ

Fig. 5

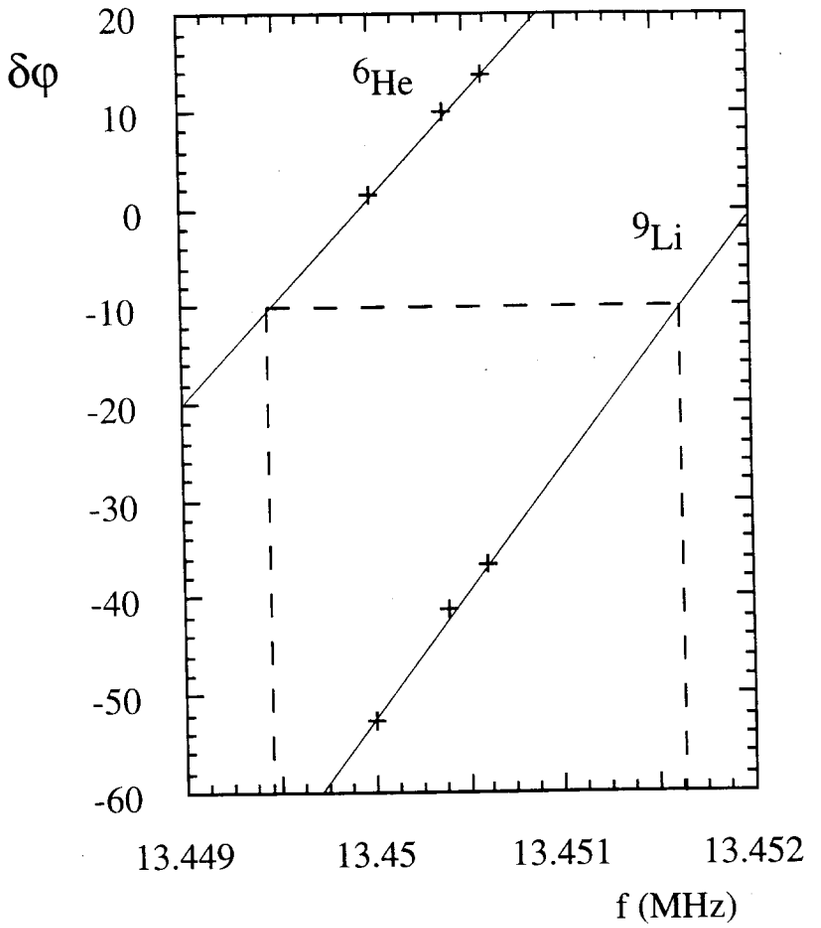

Fig. 6

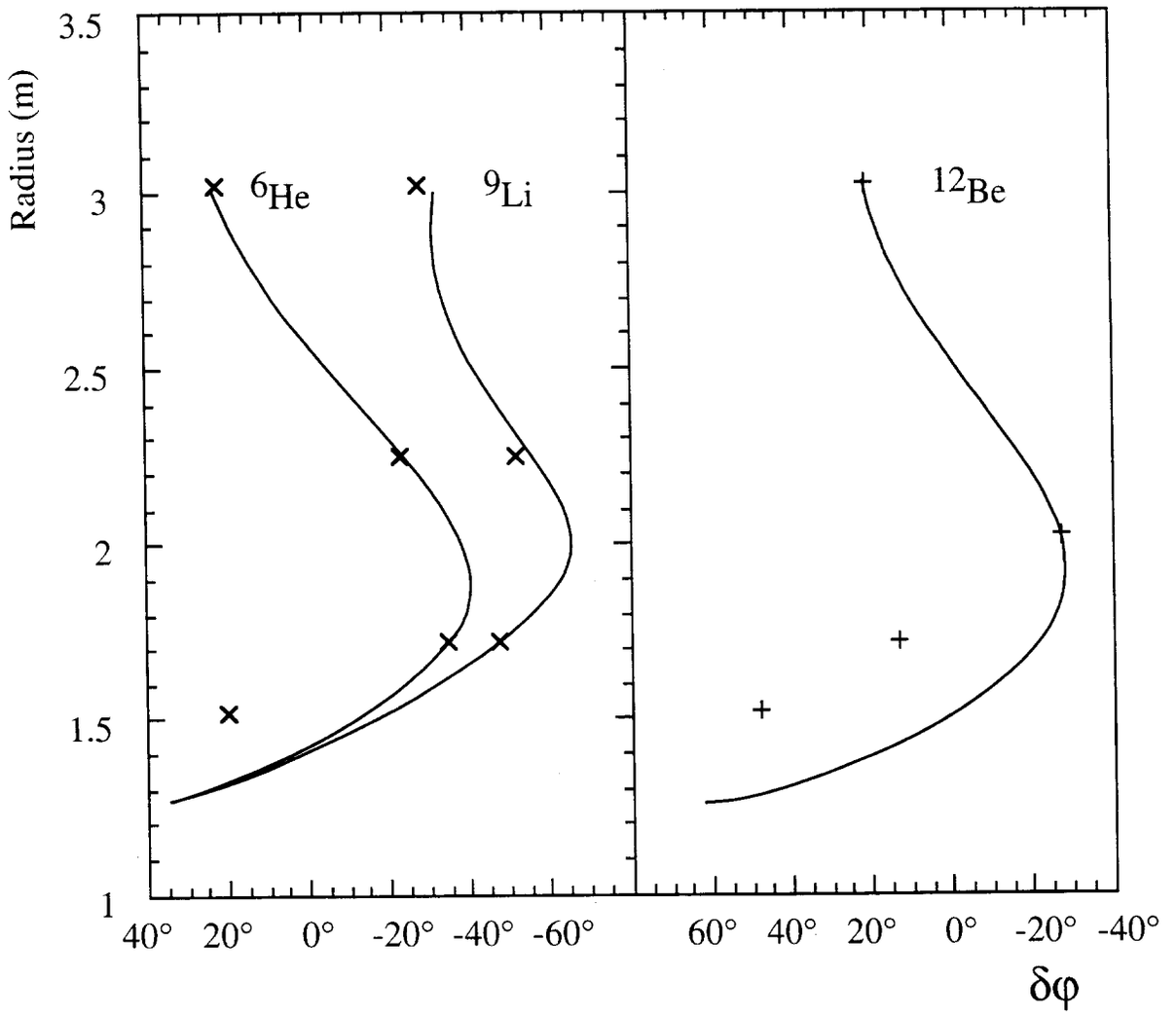
Radius (m)
3.5
3
2.5
2
1.5
1
^{6}He
^{9}Li
^{12}Be
40° 20° 0° -20° -40° -60°
60° 40° 20° 0° -20° -40°
δφ

Fig. 7

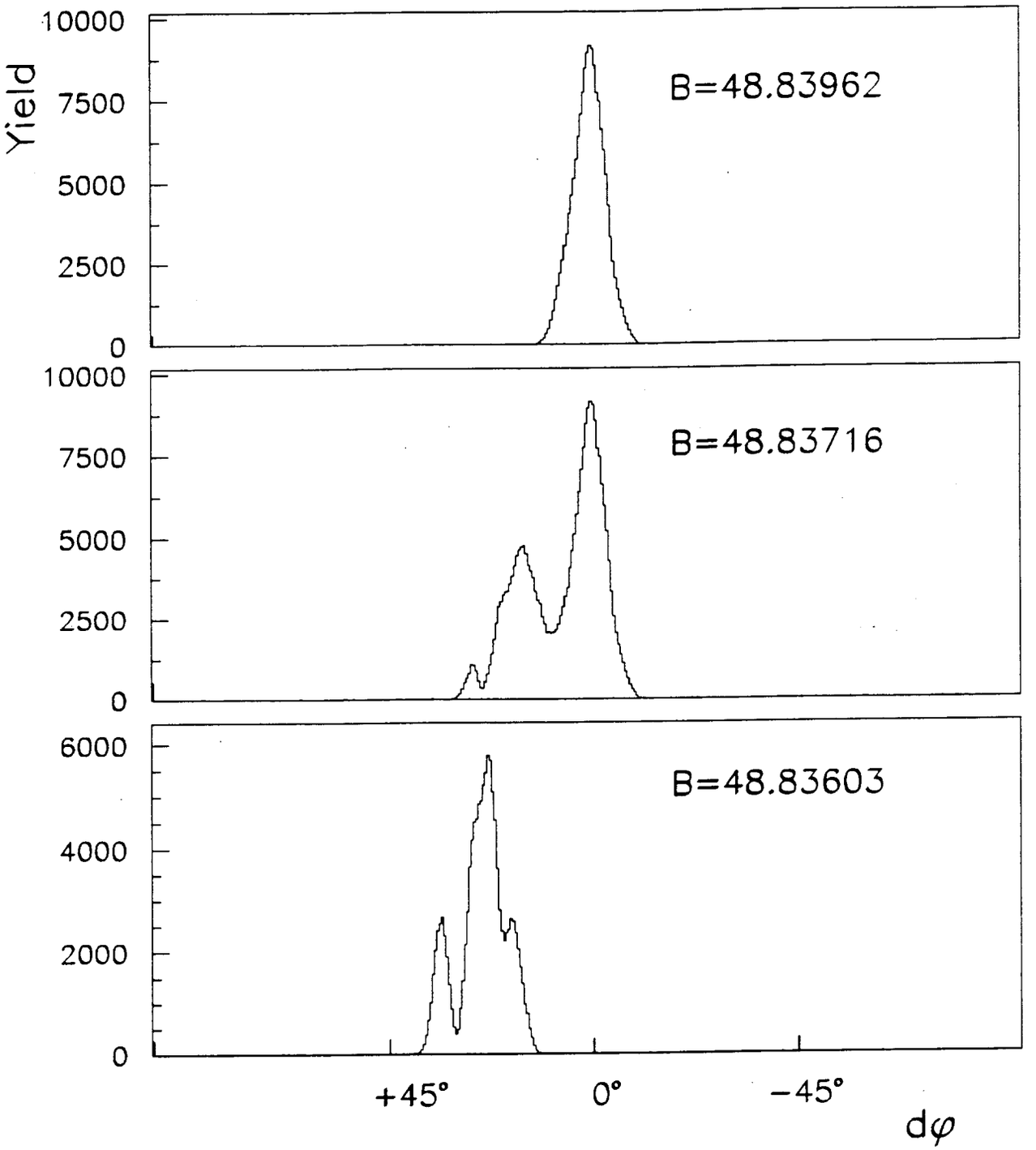
Yield
10000
7500
5000
2500
0
B=48.83962
10000
7500
5000
2500
0
B=48.83716
6000
4000
2000
0
B=48.83603
+45°
0°
−45°
dφ

Fig. 8

9 Table Captions

Table I. The tabulated atomic mass excesses $(\Delta)^{(21)}$ of the nuclei used in the present work and the $\frac{\delta(m/q)}{m/q}$ and corresponding uncertainties calculated using eq. (17) with respect to the reference m/q $^{15}N^{5+}$.

Table II Comparison of the experimentally measured $\frac{\delta(m/q)}{m/q}$ with the tabulated $\frac{\delta(m/q)}{m/q}$ (Table I).

${}^{Z}A^{q+}$	A	Z	q	$\Delta^{(21)}$ (MeV)	$\frac{\delta(m/q)}{m/q}$
${}^{15}N$	15	7	5	0.1010 ± 0.0002	$0.00000000 \pm 0.00000001$
${}^{12}B$	12	5	4	13.3690 ± 0.0014	$0.00118899 \pm 0.00000012$
${}^{12}Be$	12	4	4	25.077 ± 0.015	$0.00223672 \pm 0.00000134$
${}^{9}Li$	9	3	3	24.9540 ± 0.0019	$0.00296986 \pm 0.00000023$
${}^{6}He$	6	2	2	17.5941 ± 0.001	$0.00314140 \pm 0.00000018$

${}^{Z}A^{q+}$	$\frac{\delta B}{B}=(\frac{\delta(m/q)}{m/q})_{exp}$ (10^{-5})	$(\frac{\delta(m/q)}{m/q})_{table}$ (10^{-5})	δ_{exp}-δ_{table}
${}^{12}B^{4+}$	121.66	118.899 ± 0.009	$2.7 \cdot 10^{-5}$
${}^{12}Be$	227.48	223.672 ± 0.134	$3.8 \cdot 10^{-5}$
${}^{9}Li$	302.306	296.986 ± 0.024	$5.3 \cdot 10^{-5}$
${}^{6}He$	319.408	314.140 ± 0.016	$5.3 \cdot 10^{-5}$
${}^{6}He$-${}^{9}Li$	17.1014	17.1005 ± 0.029	$9 \cdot 10^{-9}$